Vishal Tandon[1]
Sharath K. Bhagavatula[2]
Brian J. Kirby[3]

[1]Department of Biomedical Engineering, Cornell University, Ithaca, NY, USA
[2]School of Electrical and Computer Engineering, Cornell University, Ithaca, NY, USA
[3]Sibley School of Mechanical and Aerospace Engineering, Cornell University, Ithaca, NY, USA

Received January 14, 2009
Revised March 18, 2009
Accepted March 29, 2009

Research Article

Transient ζ-potential measurements in hydrophobic, TOPAS microfluidic substrates

We utilize time-resolved electrokinetic measurements in order to study the electrokinetic properties of silica and TOPAS microfluidic channels as a function of the time history of the fluid–solid interface. In pressure-driven flow through TOPAS microchannels, the ζ-potential as inferred from streaming potential measurements decays exponentially by a factor of 1.5 with a characteristic decay time of 3 h after the initial formation of the fluid–solid interface. A similar exponential decay is observed immediately after water is exchanged for ethanol as the solvent in the system. In electroosmotically driven flow through TOPAS microchannels, the ζ-potential as inferred through current monitoring experiments was constant in time. No electrokinetic transients were observed in silica microchannels under these flow conditions.

Keywords:
Electrokinetic / Electroosmosis / Hydrophobic / Transient / ζ-potential
DOI 10.1002/elps.200900028

1 Introduction

Polymers are increasing in popularity for microfluidics applications because of their low cost, ease of fabrication, and often favorable optical and chemical properties [1–4]. Many polymers are hydrophobic, however, and the material properties of hydrophobic polymers relevant to electroosmosis are in dispute; some have reported that electrokinetic actuation in hydrophobic polymers is impossible or unpredictable [5–7], whereas others have measured significant ζ-potentials in hydrophobic substrates [1, 8–13]. The challenge in modeling and measuring electrokinetic phenomena in hydrophobic substrates stems from a poor understanding of the surface chemistry of water–hydrophobe interfaces [13]. The uncertainty in the material properties of hydrophobic substrates limits predictive capabilities for device design, and complexities arising from poorly understood interfacial phenomena can lead to poor repeatability and accuracy of experiments.

Significant scatter is observed in existing electrokinetic data for polymers [12] since these phenomena are difficult to measure and can be very sensitive to surfactants. In general, precise descriptions of electrokinetic phenomena require careful understanding of (i) the origin of interfacial charge, (ii) well-defined fluid velocity boundary conditions, and (iii) models for diffuse and condensed ion distributions [14]. Hydrophobic substrates are particularly challenging because the origin of charge is unknown, and uncertainty regarding slip leads to poorly defined fluid velocity boundary conditions [15, 16]. In addition, molecular dynamics simulations are challenging because of the aqueous solutions involved; long-range electrostatic interactions between water molecules limit both the number of simulated molecules as well as the duration of the simulation [17–24].

Some of the complexity in understanding the origin of charge in hydrophobic electrokinetic systems arises from the molecular/supramolecular structure of water at the fluid–solid interface [16]. Postulated structures include regions of reduced or depleted water density [19, 25, 26], ice-like hydrogen-bonded water molecule networks [19, 22, 27], and nanobubbles [28]. Depletion layers and water molecule networks impact ion adsorption onto the fluid–solid interface, and are therefore important factors in understanding the origin of charge. Nanobubbles are of particular interest, since their presence would affect both interfacial charge formation and the fluid mechanical boundary condition, and their thermodynamic instability [15, 28–31] could lead to unpredictable or fluctuating electrokinetic behavior in hydrophobic systems. This suggests that electrokinetic properties of hydrophobic systems may depend on the time history of the interface.

In this study, we use time-resolved electrokinetic measurements in order to study the behavior of hydrophobic microfluidic systems as a function of the time history of the interface after initiating (i) pressure-driven flow, (ii) electroosmotic flow, and (iii) exchanges between ethanol and water as the solvent in the system. We then compare those results with hydrophilic microfluidic systems. In the past, electrokinetic measurements in hydrophobic systems have been shown to be repeatable and predictable when the

Correspondence: Dr. Brian J. Kirby, Cornell University – Sibley School of Mechanical and Aerospace Engineering, 238 Upson Hall, Ithaca, NY 14853, USA
E-mail: bk88@cornell.edu
Fax: +1-607-255-1222

© 2009 WILEY-VCH Verlag GmbH & Co. KGaA, Weinheim

fluid–solid interface has reached a sufficient equilibrium [12, 13]. Through time-resolved measurements, we look to determine (i) if the time-scale for equilibration differs in hydrophobic and hydrophilic systems, (ii) whether the behavior of the system during the approach to equilibrium is erratic or deterministic, and (iii) how different flow conditions affect the equilibration time.

2 Materials and methods

2.1 Methodology

Here we model electrokinetics by assuming that interfacial phenomena lead to charge separation at fluid–solid interfaces, resulting in a double layer and a charge distribution that can be described by a Gouy–Chapman model [32]. In this context, it is sufficient to treat the ion distribution in the diffuse part of the double layer in the Boltzmann limit, where ions are considered to be point particles experiencing a bulk electrical potential, which has the value ζ at the wall. The electrical potential distribution is then given by the Poisson–Boltzmann equation:

$$\nabla^2\psi = -\frac{\rho_e}{\varepsilon} = -\frac{1}{\varepsilon}\sum_i C_{o,i} z_i F \exp\left(-\frac{z_i F}{RT}\psi\right) \quad (1)$$

where ψ is the electrical potential, ε is the permittivity of the fluid medium, z_i is the valence of the i-th ionic species, R is the gas constant, F is Faraday's constant, and $C_{o,i}$ is the concentration (moles/m^3) of the i-th species at a location where $\psi = 0$. This ion distribution leads to electroosmosis when subjected to a transverse electric field, and streaming potential when subjected to a pressure-driven flow, which we use to study electrokinetics at hydrophobic interfaces. Non-dimensionalization of the Poisson–Boltzmann equation leads to a length scale that describes the spatial extent of the double layer, the Debye length.

$$\lambda_D = \sqrt{\frac{\varepsilon RT}{2F^2 I}} \quad (2)$$

Here I is the ionic strength of the solution in moles *per* cubic meter.

In electroosmosis, an external electric field is applied to a fluid in a microchannel with a net unbalanced ion distribution as in Eq. 1, resulting in bulk flow. If the channel is straight and homogeneous, its dimensions are large as compared with the Debye length, and there are no pressure gradients, the flow is approximated as being uniform. The bulk flow velocity, u_{EO}, is then given by the Smoluchowski equation,

$$u_{EO} = -\frac{\varepsilon\zeta}{\eta}E \quad (3)$$

where η is the fluid viscosity, and E is the applied electric field. In Eq. 3, we assume that fluid properties are uniform, and that the no-slip fluid boundary condition applies precisely at the wall, at which $\psi = \zeta$. In electroosmotic flow, we infer values for the ζ-potential from measurements of the electroosmotic velocity, where ζ represents the electrical boundary condition at the fluid–solid interface in the Gouy–Chapman model. The precise physical relationship between the inferred ζ-potential and the interfacial charge at the wall is complicated and in dispute [14, 33]. In this article, we focus on experimental measurements of u_{EO} and do not address double layer models *per se*.

An imposed pressure-driven flow in a microchannel with an ion distribution described by Eq. 1 results in the bulk redistribution of unbalanced charges, and the equilibrium condition if there is no net electrical current coincides with an electrical potential called the streaming potential. The streaming potential, $\Delta\phi$, is given by

$$\Delta\phi = \frac{\varepsilon\zeta}{\eta\sigma}\Delta P \quad (4)$$

where $\Delta P = P_{\text{downstream}} - P_{\text{upstream}}$ is the applied pressure difference, and σ is the bulk fluid conductivity. Equation 4 uses the Debye–Hückel approximation, and assumes a thin double layer as compared with the channel radius, so that channel geometry effects are unimportant. Fluid conductivity is assumed to be uniform, and surface conductivity is neglected since the microchannels used in this study are relatively large (the surface conductivity is negligible compared with the bulk conductivity; this assumption leads to an error of less than 1%). In pressure-driven flow, we use streaming potential measurements to infer values for the ζ-potential.

In order to compare experiments conducted with solutions of different ionic strengths, we normalize our ζ-potential data by $pC = \log C$, where C is the counterion concentration in moles *per* liter, as described in [34].

2.2 Chemical reagents and capillaries

All reagents were obtained from Sigma-Aldrich (St. Louis, MO). Phosphate buffer solutions were prepared from stock solutions of monobasic and dibasic potassium phosphate. Solution conductivity and pH measurements were conducted using a dual pH/conductivity meter (Mettler Toledo SevenMulti, Columbus, OH) with specialized electrodes (Mettler Toledo Inlab 730 and Inlab 413, Columbus, OH) prior to each experiment, and buffers were checked periodically to ensure that there were no pH or conductivity changes over time. Solution pH was adjusted by titration with hydrochloric acid and/or sodium hydroxide. All buffers were at room temperature ($T = 25^\circ$C) for all of our experiments.

Silica and TOPAS were chosen as model hydrophilic and hydrophobic systems for this study, respectively. Silica capillaries were acquired from Polymicro Technologies (Phoenix, AZ) and TOPAS capillaries were acquired from Paradigm Optics (Vancouver, WA). TOPAS (manufactured by Zeon Chemicals, Louisville, KY) is a cyclo olefin copolymer thermoplastic that has similar properties to Zeonor, but is manufactured with less stringent processes

© 2009 WILEY-VCH Verlag GmbH & Co. KGaA, Weinheim

[http://www.topas.com/topas_brochure_english.pdf]. Both capillaries had outer and inner diameters of 360 and 25 μm, respectively. A fresh section of capillary was used in each trial of each experiment.

2.3 Automated current monitoring

An automated current monitoring method was used to measure the ζ-potential under electroosmotic flow conditions [35, 36]. For our current monitoring experiments, 250–600V was applied simultaneously across four 5-cm length microchannels using platinum electrodes and an eight-channel high-voltage sequencer (LabSmith HVS448, Livermore, CA). The sequencer was carefully calibrated prior to experiments to ensure consistent readings across channels in both forward and reverse polarity operation. Reservoirs (1.5 mL in volume) at each end of a particular microchannel contained phosphate buffer solutions that varied in conductivity by 7.5%. Control signals were implemented in LabView, where four channels in the sequencer were used to apply voltage, and four were used to monitor the current through the microchannels. Square–wave electric field sequences were applied so as to displace fluid in one direction during the first half-cycle, then in the opposite direction during the second half-cycle. The square–wave periods were designed so as to allow electroosmosis to completely displace the fluid within the microchannels during each half-cycle. Voltage was controlled *via* LabView so as to maintain the electric field across the microchannels constant during displacement.

The resulting current waveforms (Fig. 1) were analyzed in one-period segments by taking advantage of the characteristic trapezoidal profile (Fig. 2). First, we subtracted the mean (I_{mean}) from the waveform ($I(t)$), and then took its absolute value. We then integrated the resulting function over one period, τ, in order to get the area under the curve.

$$A = \int_0^{\tau} |I(t) - I_{mean}|\, dt \tag{5}$$

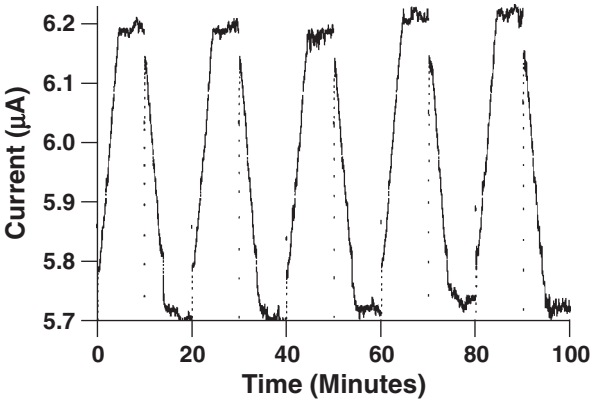

Figure 1. Example of a current monitoring raw data trace. For this data, 10 mM, pH 7, phosphate buffer was used in a silica capillary.

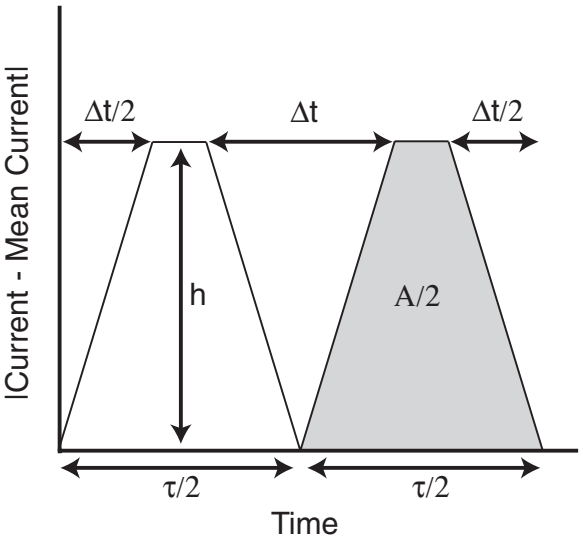

Figure 2. Schematic showing how current monitoring data were converted into a velocity measure using a trapezoidal profile.

The area, *A*, is simply the area of the two trapezoids in Fig. 2. The displacement time (the time it takes for the current signal to change from a constant high value to a constant low value and *vice versa*), Δ*t*, is then related to *A* as in

$$\Delta t = \tau - \frac{A}{h} \tag{6}$$

where *h* is the height of the trapezoids, or the maximum value of the function ($|I(t) - I_{mean}|$). Dividing the length of the microchannel, *L*, by Δ*t* then gives the electroosmotic velocity,

$$u_{EO} = \frac{L}{\Delta t} \tag{7}$$

which is converted into a ζ-potential value using Eq. 3.

Joule heating was avoided in the system by measuring electroosmotic mobility as a function of electric field magnitude and extrapolating to the zero-field limit. Only fields that produced mobilities that were within 5% of the zero-field limit were used for this extrapolation. Any temperature change due to Joule heating would also result in readily detectable changes in the mean current, and any data in which the mean current varied by more than 10% were not used. Velocity errors due to any pressure imbalances between reservoirs were removed in post-processing by averaging the data from the positive and negative half cycles in each period of the square–wave input. Errors due to the conductivity difference between the two solutions were neglected, as they were small (<1%) as compared with other uncertainties. The ζ-potential was calculated from velocity data using the Smoluchowski Equation (Eq. 3).

2.4 Phase-sensitive streaming potential

Phase-sensitive streaming potential experiments were used to measure the ζ-potential under pressure-driven flow

© 2009 WILEY-VCH Verlag GmbH & Co. KGaA, Weinheim

conditions. Pressure (0–103 kPa) was applied to the inlet of a 5 cm capillary composed of the material under study using a push/pull syringe pump (KD Scientific, Holliston, MA). Sinusoidal pressure waveforms were established *via* LabView control of syringe actuation utilizing a PID controller corrected for the pressure dependence of the system's pressure–displacement response. Pressure at the capillary inlet was measured by a strain-gauge-type transducer (Senso-Metrics SP70D, Simi Valley, CA). PEEK-ULTEM fittings (LabSmith, Livermore, CA) and 360 μm stainless-steel tubing were used to make the fluidic connections between the syringe, capillary, electrodes, and pressure transducer [37]. A 10 TΩ electrometer (6514 Electrometer, Keithley, Cleveland, OH) and platinized platinum electrodes were used to measure the generated voltage across the capillary (Fig. 3). Platinized platinum electrodes were fabricated using an electrochemical reaction as described in [38]. The platinizing solution consisted of 3.5% w/v hydrogen hexachloroplatinate, 0.005% w/v lead acetate, and 2.5% v/v 1 M HCl solution. The working platinum electrode was immersed in the platinizing solution against a counter electrode, and a potential of 7 V was applied for 120 s, resulting in a macroscopically black (platinized) platinum electrode. These electrodes have a porous structure that increases their effective surface area by orders of magnitude, vastly reducing systematic errors associated with the polarization of normal platinum electrodes. Electrodes were visually inspected in order to check for degradation prior to each experiment.

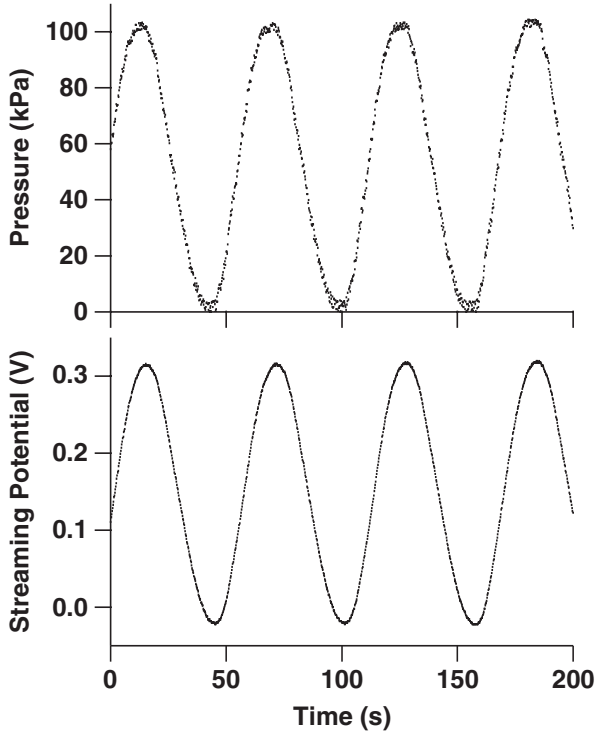

Figure 3. Example of raw streaming potential data. For this data, 1 mM, pH 7, phosphate buffer was used in a TOPAS capillary.

Forcing pressures and capillary diameters were chosen such that the flow was laminar in all cases (Reynolds number below 1200), and hydrodynamic starting lengths could be ignored. Streaming potential data that did not correlate with the applied pressure waveform generally corresponded to the presence of an air bubble in the microchannel, and were rejected. The measured pressure and streaming potential waveforms were Fourier processed and the response at the fundamental mode was measured. The ζ-potential was then calculated from Eq. 4 as follows:

$$\zeta = \frac{\eta\sigma}{\varepsilon}\frac{\Im\{\phi(t)\}}{\Im\{\Delta P(t)\}}\bigg|_{f=f_0} \tag{8}$$

where $\Im$ denotes the discrete Fourier transform, and f_0 is the frequency of the fundamental mode, *i.e.* the driving frequency of the pressure waveform. Errors due to surface conductivity, non-Debye–Hückel charge distributions and wall curvature were ignored as they were small as compared with conductivity and temperature uncertainties, which were on the order of 10%. Since Eq. 4 holds strictly at equilibrium, the period of the applied pressure waveform was chosen to be slow enough (120 s) so as to allow for a quasi-static measurement. If the system is not allowed to reach equilibrium, there will be a phase lag between the streaming potential waveform and the pressure-driven waveform. The damping of the streaming potential waveform magnitude that occurs in a system with a phase lag can be corrected for if the phase lag is simultaneously measured:

$$\zeta = \zeta_0(1 + \tan^2\alpha) \tag{9}$$

where ζ_0 is the uncorrected ζ-potential, and α is the phase difference between the streaming potential and pressure waveforms. The phase lag, however, was negligible in all of our experiments.

3 Results

We conducted experiments in both hydrophobic, TOPAS microfluidic channels and hydrophilic, silica microchannels in order to measure their electrokinetic properties as a function of the time history of the fluid–solid interface. In particular, we measured the ζ-potential as a function of time (i) in pressure-driven flow inferred from streaming potential measurements, (ii) in electroosmotic flow inferred from current monitoring experiments, (iii) in pressure-driven flow after an initial exposure to an electric field, and (iv) after exchanging ethanol as the solvent in the system for water.

3.1 Time-resolved electrokinetic measurements in pressure-driven flow

We measured the ζ-potential as a function of time after filling with aqueous solution in both hydrophobic (TOPAS) and hydrophilic (silica) microchannels under pressure-driven flow, utilizing the phase-sensitive streaming potential

© 2009 WILEY-VCH Verlag GmbH & Co. KGaA, Weinheim

technique. In both materials, we flushed a pH 7, 1 mM phosphate buffer solution through the microchannels using an applied pressure sinusoidally varying from 0 to 103 kPa (gauge), with a period of 120 s. In TOPAS, we also measured the ζ-potential for a 10 mM, pH 7, phosphate buffer solution with the same pressure–wave parameters. The resulting sinusoidal streaming potential signals were monitored continuously and recorded with a sampling rate of 5 Hz for 10 h. The applied pressure and resulting streaming potential waveforms were analyzed in 12-min segments using Eq. 4 to give an inferred ζ-potential as a function of time.

In the TOPAS microchannels filled with 1 mM phosphate buffer, the normalized ζ-potential was initially high in magnitude at −25 mV, but decayed to an equilibrium value of −16.1 mV (Fig. 4A). The transient is well fit by an exponential decay, with a time constant of 3.0 h. The normalized ζ-potential for 10 mM phosphate buffer in TOPAS had a very similar exponential decay, with an equilibrium value of −16.0 mV and a time constant of 2.7 h (Fig. 4B). ζ/pC in the silica microchannels, on the other hand, was constant over the 10-h period (Fig. 4C), with a time average of −27.0 mV that varied by less than 3% for the duration.

When the phosphate buffer solution was allowed to equilibrate with the TOPAS microchannels for 5 h prior to a streaming potential measurement, ζ/pC decayed exponentially from −16.8 to −13.9 mV over the next 10 h, with a time constant of 2.1 h (Fig. 5). A comparison of our ζ/pC *versus* time data for 0–10 h after flushing with our data for 5–15 h after flushing shows that the two trends are consistent during the overlap period (5–10 h), though the time constants for the exponential decays are slightly different.

3.2 Time-resolved electrokinetic measurements in electroosmotic flow

We conducted time-resolved measurements of the ζ-potential in both hydrophobic TOPAS and hydrophilic silica microchannels under electroosmotic flow using the current monitoring technique. For the measurements of the electrokinetic properties of TOPAS, an electric field magnitude of 120 V/cm was applied across the microchannel for a half-cycle period of 6 min. For the silica microchannels, an electric field magnitude of 50 V/cm was used with a half-cycle period of 10 min. A 10 mM, pH 7, solution of phosphate buffer was used in both the silica and

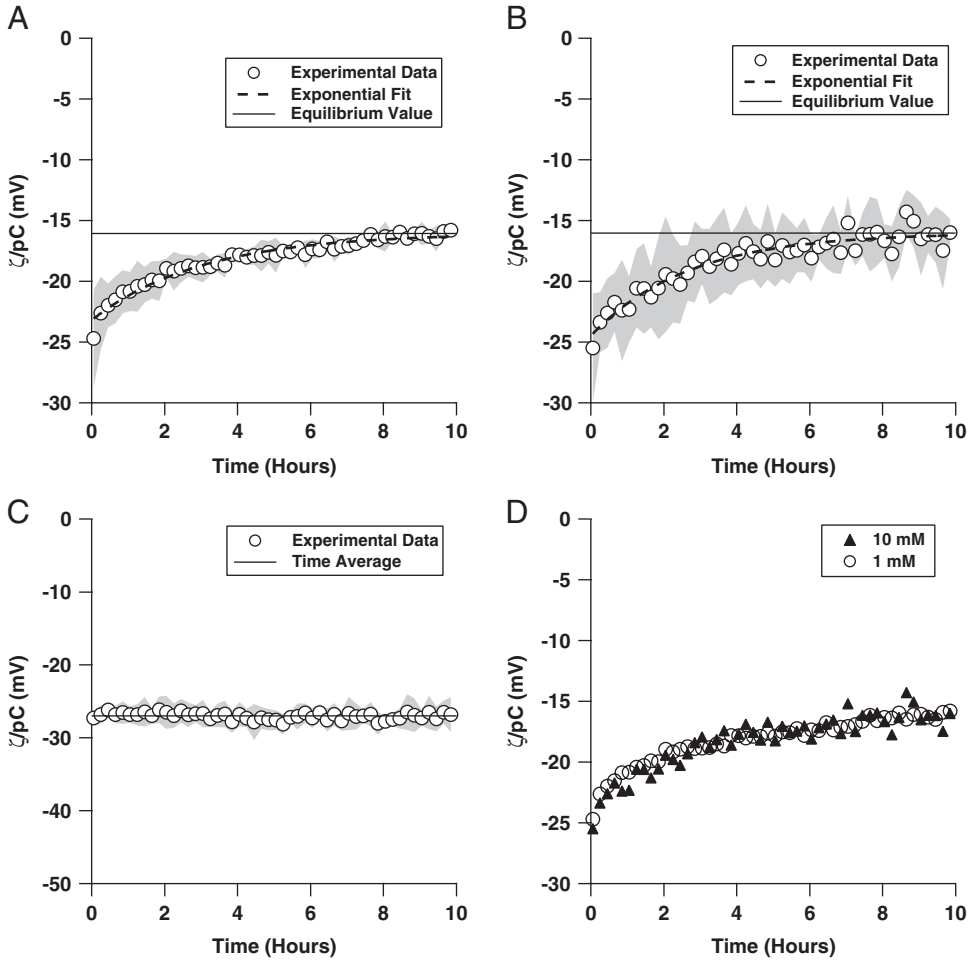

Figure 4. Normalized ζ-potential, ζ/pC, ($pC = \log C$, C is the counterion concentration expressed in molar) inferred from streaming potential measurements in pressure-driven flow, as a function of time for (A) a TOPAS microfluidic channel with 1 mM, pH 7, phosphate buffer solution (four trials), (B) a TOPAS microfluidic channel with 10 mM, pH 7, phosphate buffer solution (six trials), and (C) in a silica microfluidic channel with 1 mM, pH 7, phosphate buffer solution (four trials). In (D), the 1 mM data from (A) and the 10 mM data from (B) are compared. Data shown are an average of the independent trials, where the shaded region represents the standard deviation between the trials.

© 2009 WILEY-VCH Verlag GmbH & Co. KGaA, Weinheim

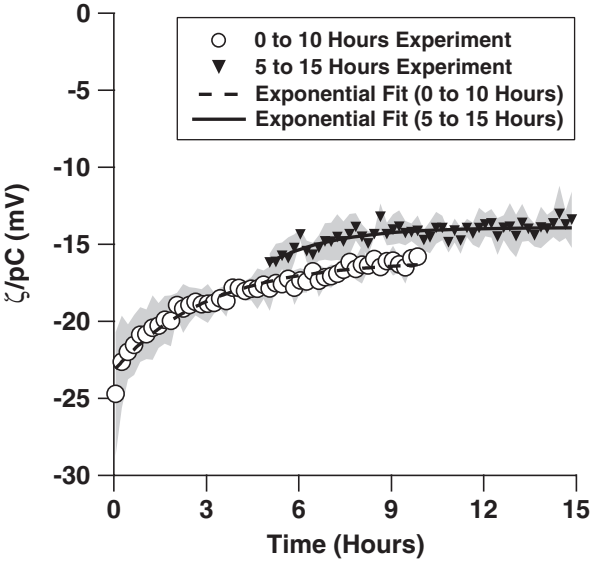

Figure 5. Normalized ζ-potential, ζ/*pC* (*pC* = log *C*, *C* is the counterion concentration expressed in molar) in a TOPAS microchannel inferred from streaming potential measurements in pressure-driven flow after 5 h of equilibration (the data were taken from 5 to 15 h after the initial filling of the microchannel). The data are compared with the direct measurement (0–10 h, Fig. 4A). A 1 mM, pH 7, phosphate buffer solution was used, and the data shown are an average of four independent trials, where the shaded region represents the standard deviation between the trials.

the TOPAS experiments. In contrast to our experiments in pressure-driven flow, the ζ-potential in both TOPAS and silica was constant and varied by less than 7% over a period of 10 h (Fig. 6). The time-averaged value of the normalized ζ-potential, ζ/*pC*, for TOPAS was −14.1 mV with a standard deviation of 1.0 mV or 7%. The time average of ζ/*pC* in silica was −25.7 mV with a standard deviation of 1.6 mV or 6%.

3.3 Effect of an applied electric field on transients in pressure-driven flow

In these experiments, we examined the effect of an initially applied electric field in disrupting electrokinetic transients in pressure-driven flow. TOPAS microchannels were initially filled with a 1 mM, pH 7, phosphate buffer solution. An electric field of magnitude 500 V/cm was then applied across the microchannel for 12 min so as to actuate electroosmotic flow. The electric field magnitude was chosen so that the shear stress at the fluid–solid interface during the initial period of electroosmotic flow would be roughly a factor of 2 larger than in the current monitoring experiments (see Section 4.2, for shear stress calculations). The electric field was then switched off, flow actuated *via* a sinusoidal pressure waveform, and the streaming potential measured as described in the pressure-driven flow experiments from Section 3.1, using the same experimental parameters.

In contrast to pressure-driven flow without an initially applied electric field (Fig. 4A), the ζ-potential remained relatively constant from the time the electric field was switched off over a period of 10 h (Fig. 7). The normalized ζ-potential decayed from −17.3 to −15.1 mV, and had a time average of −15.9 mV, with a standard deviation of 0.8 mV or 5%. The variation is not explained by an exponential decay, as an exponential fit to the data in Fig. 7 resulted in a nonsensical time constant and a low R^2 value. The data point at $t = 0$ was not used in this analysis, since one of the four

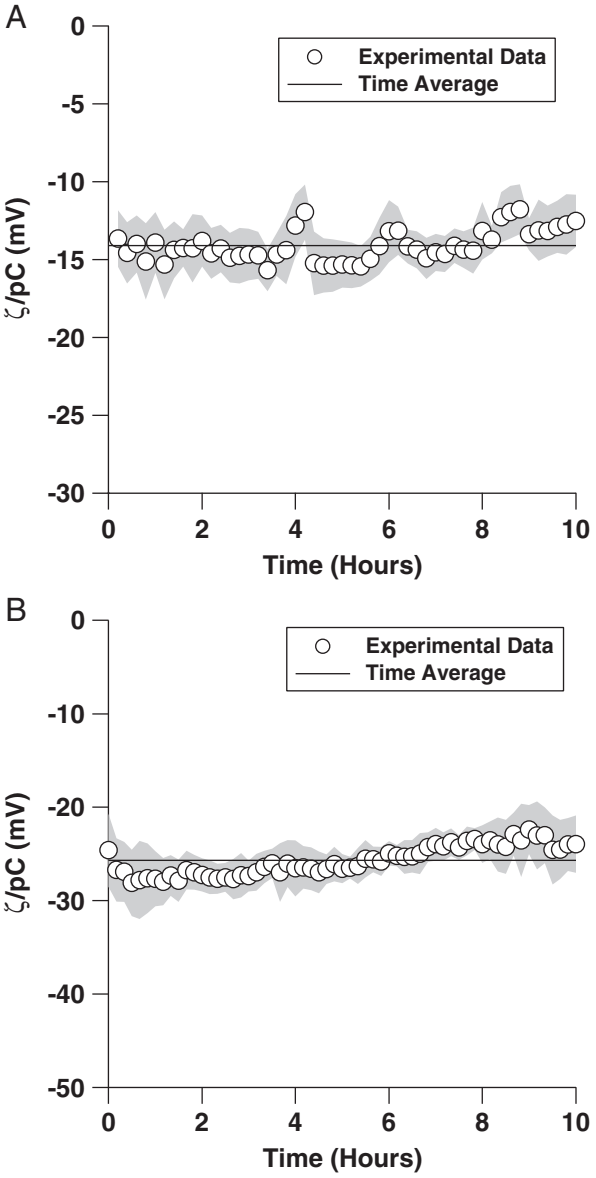

Figure 6. Normalized ζ-potential, ζ/*pC*, (*pC* = log *C*, *C* is the counterion concentration expressed in molar) in electrokinetically driven flows as inferred *via* current monitoring in (A) TOPAS and (B) silica microchannels. A 10 mM pH 7, phosphate buffer solution was used in both experiments. Data shown are an average of four independent trials, where the shaded region represents the standard deviation between the trials.

© 2009 WILEY-VCH Verlag GmbH & Co. KGaA, Weinheim

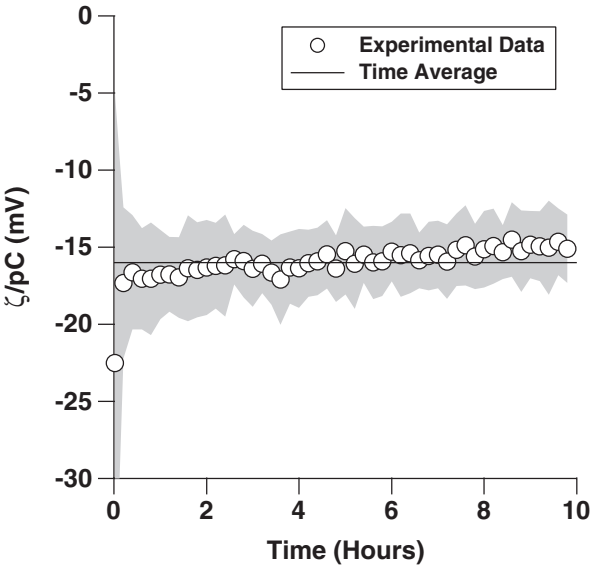

Figure 7. Normalized ζ-potential, ζ/*pC*, (*pC* = log *C*, *C* is the counterion concentration expressed in molar) as a function of time in a TOPAS microchannel under a pressure-driven flow, as inferred *via* streaming potential. Flow was initially driven through the channel electroosmotically for 12 min. A pH 7 solution with 1 mM phosphate buffer was used. Data shown are an average of four independent trials, where the shaded region represents the standard deviation between the trials.

trials for that datum was determined to be a statistical outlier by Chauvenet's criterion.

3.4 Solvent exchange experiment

Since solvent exchanges have been shown to affect the interfacial properties of water–hydrophobe interfaces [39], we conducted experiments to determine the effects of ethanol–water solvent exchanges on the electrokinetic properties of hydrophobic microfluidic channels.

In each of four trials, a TOPAS microchannel was initially filled with a solution of 90% ethanol and 10% 10 mM, pH 7, phosphate buffer (resulting in an overall counterion concentration of 1 mM). The ethanol solution was then driven through the microchannel *via* a sinusoidally varying applied pressure, with a peak magnitude of 15 psig, and a period of 120 s. The resulting streaming potential signal was monitored continuously and recorded for a minimum of 6 h. An aqueous, 1 mM, pH 7, phosphate buffer was then flushed through the microchannel, with flow actuated with the same pressure waveform, and the streaming potential monitored again for a minimum of 6 h. An additional ethanol cycle and an additional aqueous cycle followed in the same fashion. The applied pressure and resulting streaming potential waveforms were analyzed in 18-min segments using Eq. 4 to give an inferred ζ-potential as a function of time. The differences in fluid properties between the ethanol and aqueous solutions, namely the permittivity, viscosity, and conductivity, were accounted for in this analysis.

Whenever the aqueous solution replaced the ethanol solution as the solvent, there was an initial transient in which the magnitude of the apparent ζ-potential was initially high, with a normalized value of −22 mV (Fig. 8A). During the first ethanol cycle, the inferred ζ-potential changed gradually from −5.2 to −3.2 mV, but during the second ethanol cycle, the ζ-potential remained relatively constant. As was the case for the initial transients found in

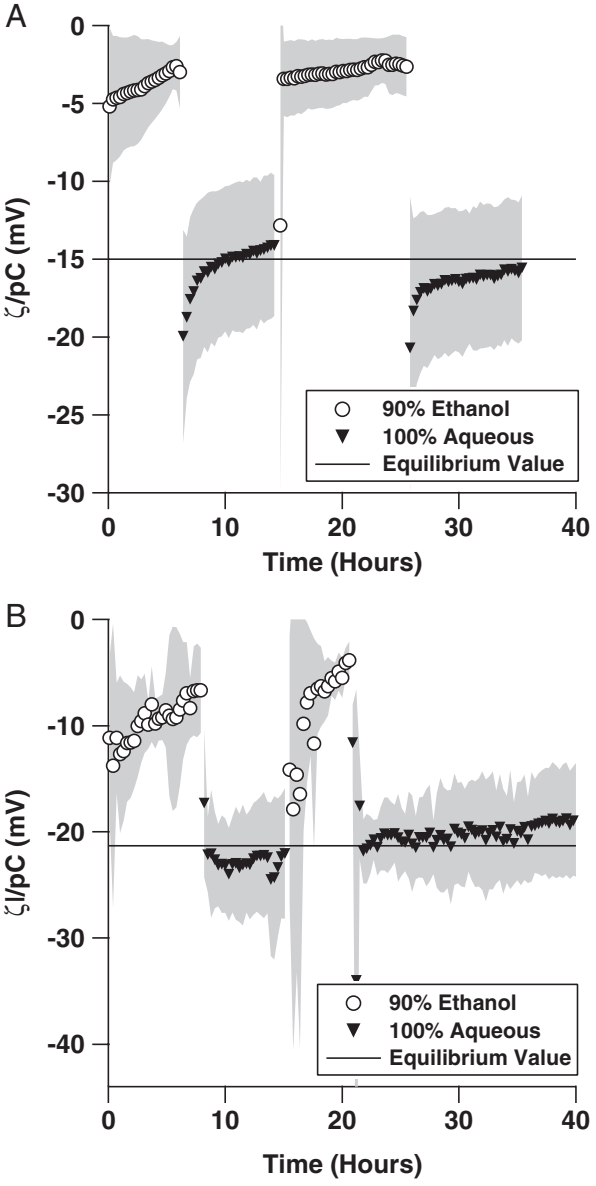

Figure 8. Normalized ζ-potential, ζ/*pC*, (*pC* = log *C*, *C* is the counterion concentration expressed in molar) as a function of time in (A) a TOPAS microfluidic channel and (B) in a silica microfluidic channel. Data shown are an average of four independent trials, where the shaded region represents the standard deviation between the trials.

© 2009 WILEY-VCH Verlag GmbH & Co. KGaA, Weinheim

pressure-driven flow, the ζ-potential magnitude variation during the aqueous cycles is well fit by exponential decays, with a normalized equilibrium value of −14.5 mV and a time constant of 1.5 h for the first aqueous cycle; −15.8 mV and 3.0 h for the second aqueous cycle.

We repeated the same experiment in hydrophilic silica microchannels in order to determine whether these transients are unique to hydrophobic systems. Similar transients were not observed during the aqueous cycles in silica microchannels (Fig. 8B). There is some variation in the inferred ζ-potential with time after the exchange from the aqueous solution to the ethanol solution, but in this case the ζ-potential gradually changes from the aqueous value to the ethanol value. ζ/pC has a mean value of −22.7 mV during the first aqueous cycle in silica, with a standard deviation of 2.8 mV (13%). During the second aqueous cycle, the mean and standard deviation are −20.0 and 2.1 mV (11%).

4 Discussion

In general, transients in the inferred ζ-potential were only observed in hydrophobic microchannels, and not in hydrophilic microchannels (Table 1). Furthermore, no transients were observed under electroosmotic flow at a field strength of 120 V/cm, or if the microchannels were initially exposed to a 500 V/cm field for only 12 min. If these transients are present in other hydrophobic substrates, they may explain much of the uncertainty in ζ-potential measurements in the literature for polymeric substrates [12], as the time history of the fluid–solid interface is rarely given careful consideration. There is significant disagreement between various ζ-potential measurements for PDMS [36, 40–44], polystyrene [10, 45, 46], polyethylene [8, 47, 48], PTFE [8, 9, 13, 49–51], and Zeonor [1, 5–7, 13], for example; in particular some have reported that Zeonor has zero electroosmotic mobility [5–7]. Schutzner and Kenndler [8] reported a decrease in the electroosmotic mobility in PTFE capillaries through subsequent experimental measurements, which is consistent with the trends we have observed in TOPAS, though those measurements were made under electroosmotic flow conditions with an applied field magnitude of 6.3 V/cm. Our experiments have shown that this decrease over time is likely to be the result of a physical phenomenon at the fluid–solid interface, and not an artifact of the measurement. By explicitly measuring the time dependence of the decay with high resolution, we have shown that the transient behavior is repeatable and predictable, and have quantified the equilibration time to be on the order of hours in TOPAS substrates. In addition to the implications of these results for experimental ζ-potential measurements, this is also important for placing molecular dynamics simulations of water–hydrophobe interfaces in context, as they typically run on very short (≪ 1 s) time-scales [17–24]. We discuss our observations in each of our specific experiments further in the following sections.

Table 1. Summary of results

	Equilibrium $\frac{\zeta}{pC}$ (mV)	Time constant (h)
Pressure-driven flow		
TOPAS (1 mM PB)	−16.1	3.0
TOPAS (1 mM PB)(After 5 h equilibration)	−13.9	2.1
TOPAS (10 mM PB)	−16.0	2.7
Silica (1 mM PB)	−27.0 ± 0.7	–
Electroosmotic flow		
TOPAS (10 mM PB)	−14.1 ± 1.0	–
Silica (10 mM PB)	−25.7 ± 1.6	–
Pressure-driven flow after EO		
Topas (1 mM PB)	−15.9 ± 0.8	–
After solvent exchange		
TOPAS (1 mM PB) – first aqueous cycle	−14.5	1.5
TOPAS (1 mM PB) – second aqueous cycle	−15.8	3.0
Silica (1 mM PB) – first aqueous cycle	−22.7 ± 1.3	–
Silica (1 mM PB) – second aqueous cycle	−20.0 ± 2.1	–

In cases where the ζ-potential is considered to be relatively constant in time, the time average with a standard deviation is listed as the equilibrium value. In those cases, exponential fits to the data produced non-sensical (extremely high or low) time constants, and low R^2 values.

4.1 Time-resolved electrokinetic measurements in pressure-driven flow

Electrokinetic transients have been studied in the context of pH hysteresis in silica [52], and electroosmotic mobilities have been reported to decrease over time in PTFE microchannels [8]. However, to the authors' knowledge, no explicit measurements of the inferred ζ-potential as a function of time with high temporal resolution have been reported. Though the inferred ζ-potential in TOPAS varied with time, the equilibrium value for ζ/pC (−16.1 mV) is in good agreement with previously reported results (−17.4 ± 4.3 mV), where channels were equilibrated with solution for 8 h before testing [13]. The normalized ζ-potential as a function of time was nearly identical for both 1 and 10 mM phosphate buffer solutions (see Fig. 4D), suggesting that the transient does not depend on the solution ionic strength in this range. The standard deviation across trials was higher for the 10 mM experiments (Fig. 4B), which is consistent with the reduced signal-to-noise-ratio due to the smaller streaming potential magnitude associated with the higher conductivity solution and the smaller ζ-potential. Furthermore, when we equilibrated the TOPAS microchannels with solution for 5 h before time-resolved measurements, the results were largely consistent with the assertion that the decay is caused by exposure to solution, not an artifact of the measurement. The equilibrium value (−13.9 mV) was again in good agreement with

© 2009 WILEY-VCH Verlag GmbH & Co. KGaA, Weinheim

previously reported results. This suggests that the transient is related to a physical equilibration phenomenon at the fluid–solid interface. Our value for ζ/pC in silica microchannels, −27.0 mV, also agrees with those from experiments found in the literature [34, 53–55], though its magnitude is at the low end of the range of reported values (Table 2) [34].

The long-time-scale decay observed here in TOPAS microchannels and previously in PTFE microchannels [8] is related to a slow equilibration process at the fluid–solid interface, and this particular form of transient is likely to be unique to hydrophobic surfaces, as similar transients were not observed in silica microchannels. The effects of a slow chemical reaction are not expected to be the cause of this, since TOPAS is chemically inert, and such a reaction is not consistent with our current monitoring data. Unexpected behavior involving impurities in the TOPAS left over from the manufacturing process is unlikely since (i) the observed trends are repeatable and predictable, as evidenced by the low standard deviation across measurements (see Fig. 4A, shaded region) and agreement with previously published results [13], (ii) no reactive impurities were found on similar Zeonor substrates [1], and (iii) impurities cannot explain the repeatability of ζ-potential measurements for a given material across substrates fabricated by different manufacturing processes [13]. Stabilization or equilibration of salt ions in the double layer does not explain the data, as 1 and 10 mM phosphate buffer solutions had transients with identical time-scales.

Nanobubbles have been observed *via* AFM to form at water–hydrophobe interfaces [28, 31, 56–59], but not at hydrophilic interfaces, and since they are thermodynamically unstable, they have a lifetime on the order of hours [28–31], which is similar to the time-scale of the transients observed in our experiments. The existence of gas at the interface would affect the boundary condition for fluid flow, and introduce apparent slip [15]. Since we infer the ζ-potential from macroscopic fluid mechanical electrokinetics experiments, slip, if present, would lead to an inflated apparent ζ-potential [16]. Thus nanobubbles are one example of a physical phenomenon at the fluid–solid interface, which is unique to hydrophobic surfaces that equilibrate on a similar time-scale to our measured electrokinetic transients.

Table 2. Comparison of ζ-potential measurements in silica microchannels at pH 7[a)]

Measurement technique	$\frac{\zeta}{pC}$ (mV)
This study, current monitoring	−25.7
This study, streaming potential	−27.0
Dickens *et al.* [55], capillary electrophoresis	−29.0
Scales *et al.* [53], streaming potential	−30.7
Kosmulski and Matijevic [54], particle electrophoresis	−32.2
Caslavska and Thormann [11], capillary electrophoresis	−40.4
Schwer and Kenndler [62], capillary electrophoresis	−52.2

a) Data are temperature corrected to 20°C, as reported in [34].

4.2 Time-resolved electrokinetic measurements in electroosmotic flow

In both the hydrophobic, TOPAS microchannels and the hydrophilic, silica microchannels, the ζ-potential was constant over time when flow was driven electroosmotically by electric fields of 120 and 50 V/cm, respectively. The ζ-potential measured for TOPAS in electroosmotic flow matches the equilibrium ζ-potential value measured from pressure-driven flow to within 14%, and with previously published results to within 23% (The standard deviation in that measurement was 25%) [13]. Our value for the ζ-potential in silica inferred from electroosmotic flow, −25.7 mV, agrees with our pressure-driven flow result to within 5%, and is at the low end of the distribution of data found in the literature (Table 2) [34, 53–55].

There are several differences between the electroosmotic flow and the pressure-driven flow experiments that may explain the presence of a transient in only the latter case including: (i) possible temperature changes due to Joule heating, (ii) differing shear stress at the fluid–solid interface due to the difference in the flow profiles, and (iii) the presence of an electric field. Temperature changes due to Joule heating do not explain the transient, as there is no current in the system during a streaming potential experiment, and any current monitoring data in which there was evidence of Joule heating was rejected. The shear stress at the fluid–solid interface was nearly an order of magnitude higher in our electroosmotic flow experiments than it was in our pressure-driven flow experiments. The shear in each of the two flow conditions is given by

$$\tau_w = \eta\left(\frac{\partial u}{\partial n}\right)_{wall} = \begin{cases} -\frac{\Delta P}{2\Delta L}R & \text{for pressure} - \text{driven flow} \\ -\frac{2RT}{F\lambda_D}\sinh\left(\frac{F\zeta}{2RT}\right) & \text{for electroosmotic flow} \end{cases} \quad (10)$$

where R is the channel radius, and the electroosmotic shear is an approximation that assumes thin double layers and a symmetric 1:1 electrolyte. In our experiments, the average shear stress in pressure-driven flow was calculated to be 13 Pa, whereas in electroosmotic flow, it was 88 Pa. Either the electric field or the increased shear stress at the wall may cause a physical change to the fluid–solid interface that disrupts the transient. If the transient is disrupted by an initial change to the system caused by the application of an electric field and the attendant electroosmotic flow, then it should be possible to disrupt the transient in pressure-driven flow by initially applying an electric field, and then measuring the ζ-potential as a function of time *via* streaming potential. We explored this further in another experiment.

© 2009 WILEY-VCH Verlag GmbH & Co. KGaA, Weinheim

4.3 Effect of an applied electric field on transients in pressure-driven flow

The transient observed in our pressure-driven flow experiments was disrupted in this case by the initial application of an electric field. The time-averaged ζ-potential is in excellent agreement with the equilibrium value from our pressure-driven flow experiments, differing by less than 2%. It is also in good agreement with our previously reported results [13], differing by less than 10%. The ζ-potential varied by only 5% from the time average over the 10 h, and in contrast to our simple pressure-driven flow experiment, the variation in this case was not well described by an exponential decay, indicating that it was essentially constant. The solution ionic strength was the same in this experiment as it was in the pressure-driven flow experiment (1 mM), and hence differing solution ionic strengths between experiments do not explain the differences in transient electrokinetic behavior. The shear stress during the 12 min of electroosmotic flow, however, was an order of magnitude larger than it was during the subsequent pressure-driven flow. During the time the electric field was applied, the shear stress was calculated from Eq. 10 to be 187 Pa. When the electric field was switched off and the flow actuated *via* pressure, the shear stress was 13 Pa, the same as it was in the pressure-driven flow experiments. The constant ζ-potential observed in this experiment demonstrates that an initial period of electroosmotic flow disrupts the transient, which is consistent with our hypothesis that exposure to an electric field with the attendant higher shear stress at the wall causes a physical change at the fluid–solid interface that affects the electrokinetic properties of the system. Future experiments with high-shear pressure-driven flow may allow for the shear and electric field effects to be decoupled.

4.4 Solvent exchange experiment

In this set of experiments, we demonstrated that we can induce transients in the electrokinetic response of a hydrophobic microfluidic channel by replacing ethanol as the solvent in the system for water. Since the solubility of air is higher in ethanol than it is in an aqueous solution [60], replacing ethanol with water is expected to result in the evolution of gas, some of which is trapped at the fluid–solid interface in the form of nanobubbles. The generation of such nanobubbles after ethanol–water solvent exchanges has been demonstrated on OTS–slicon surfaces *via* tapping mode AFM microscopy [39]. Since the nanobubbles are unstable and impact the chemical and fluid boundary conditions for the system, the solvent exchanges are expected to lead to observable changes in the electrokinetic behavior of microfluidic systems.

During the aqueous cycles of the the solvent exchange experiment in TOPAS, the equilibrium values for ζ/pC (−14.5 and −15.8 mV) were essentially the same as those observed in pressure-driven flow with no solvent exchanges (−16.1 mV, see Table 1), differing by less than 11% in both cycles. They also match both the nearly constant ζ-potential magnitude observed in electroosmotically driven flow (−14.1 mV), as well as the value from previously published results (−17.4 mV) [13]. As was the case in our pressure-driven flow experiments, the transients during the aqueous cycles here were well described by exponential decays with time constants on the order of hours. As before, the transients are not likely to have been caused by a slow, reversible chemical reaction with the substrate or with impurities, since TOPAS is non-reactive and the transients were consistent across multiple trials (See Fig. 8A, where the shaded region indicates variation across trials). Furthermore, the transients were regenerated after a second solvent exchange, discounting the possibility of a permanent chemical modification to the surfaces.

In the silica microchannels, the same transients were not observed during the aqueous cycles. There was some time dependence of the ζ-potential when the aqueous solution was exchanged for ethanol, but in this case the ζ-potential gradually changed from the aqueous value to the ethanol value, which may be indicative of a period of time in which there was a mixture of both solutions in the microchannel. The high standard deviation immediately following the exchange from the aqueous solution to ethanol (shaded region, Fig. 8B) also suggests that the fluctuation could be due to experimental error. This is in sharp contrast to the TOPAS microchannel, where upon changing from ethanol to water, the ζ-potential magnitude initially increased by 67% over the equilibrium value, and the standard deviation was nearly constant throughout the aqueous cycle. This large increase cannot be explained by a simple transition period involving a mixture of the two solvents. The constant ζ-potential values measured during the aqueous cycles in silica are in good agreement with data from our other experiments and the data found in the literature (Table 2) [34, 53–55]. Solvent exchanges led to transients in hydrophobic TOPAS microchannels, whereas in hydrophilic silica microchannels, they did not.

Given the evidence for nanobubble formation on hydrophobic surfaces after ethanol–water solvent exchanges [39], a similar solvent exchange in our TOPAS microfluidic system is also likely to generate nanobubbles at the fluid–solid interface. The nanobubbles are thermodynamically unstable [15, 28–31, 61] owing to their small size (∼10 nm in radius). The Young–Laplace pressure inside a bubble 10 nm in radius is on the order of 144 atm, and as such the bubbles are expected to dissipate nearly instantaneously [13, 15, 61]. On a hydrophilic surface, any nanobubbles that form do indeed dissipate instantaneously, as nanobubbles have not been observed on hydrophilic surfaces [56], and we did not observe any electrokinetic transients in hydrophilic, silica microchannels. In a hydrophobic system, on the other hand, nanobubbles have been shown to have longer than expected lifetimes (on the order of hours) [28–31], due to a reduction in total free energy afforded by low surface tension between the gas and the hydrophobic surface. The

© 2009 WILEY-VCH Verlag GmbH & Co. KGaA, Weinheim

existence of nanobubbles on the surface introduces a local slip boundary condition due to the presence of a low viscosity gas layer near the surface. In a simple 1-D approximation, the slip length, b, is given by

$$b = h\left(\frac{\eta_1}{\eta_2} - 1\right) \tag{11}$$

where h is the height of the nanobubble, η_1 is the viscosity of the liquid phase, and η_2 is the viscosity of the gas phase [15]. For a bubble 10 nm in height, Eq. 11 gives a slip length of 0.55 μm. Slip leads to an increase in the apparent ζ-potential, ζ_a, given by the following expression in the Debye–Hückel, thin double layer limit [16].

$$\zeta_a = \zeta\left(1 + \frac{b}{\lambda_D}\right) \tag{12}$$

Equation 12 predicts that in a 1 mM phosphate buffer solution, slip due to nanobubbles can lead to an apparent ζ-potential that is a factor of 57 larger than the actual ζ-potential. It should be noted, however, that nanobubbles are not expected to cover the entire surface, and there is recirculating flow within the nanobubbles [16], and hence Eq. 11 overestimates the slip length. In this experiment, the ζ-potential after solvent exchange was only 1.5 times larger than the equilibrium value. It is expected that nanobubble dissolution over time leads to a reduction in the effective macroscopic slip length, leading to a decay in apparent ζ-potential. Thus, the lifetime of nanobubbles in a hydrophobic, TOPAS microfluidic system after ethanol–water solvent exchanges is expected to coincide with the time-scale of our observed electrokinetic transients. Further experiments involving direct observation of nanobubble populations as a function of time with AFM are necessary in order to explore this link further.

5 Concluding remarks

We have demonstrated that the electrokinetic properties of hydrophobic, TOPAS microfluidic substrates depend on the time history of the fluid–solid interface. In flow driven by a 20.2 kPa/cm pressure gradient, there is an initial transient where the inferred ζ-potential is initially high in magnitude immediately following formation of the interface, and it ultimately decays to an equilibrium value. Such a transient is not present in hydrophilic, silica microchannels. This decay is a function of time elapsed after interface formation and not experimental measurement time. This indicates that the transient is related to a physical phenomenon at the interface, and that the equilibrium is only a function of time, and not the measurement parameters or apparatus. There is no transient in either TOPAS or silica under electroosmotic flow. However, if a TOPAS microchannel is exposed to an initial short period of electroosmotic flow prior to a pressure-driven flow, the inferred ζ-potential is constant in time. The initial application of an electric field results in a rapid equilibration of the interface, disrupting the transient. Furthermore, we have shown that we can generate similar transients in TOPAS microchannels by replacing ethanol as the solvent in the system with water. A similar solvent exchange does not result in transients in hydrophilic, silica substrates. These transients are also likely caused by a physical equilibration phenomenon at the interface, but are not caused by a permanent chemical change, since they can be induced repeatedly by subsequent solvent cycling between water and ethanol. It is also unlikely that slow, reversible chemical reactions can explain these transients, since the TOPAS substrate is chemically inert.

Future work will focus on quantifying the possible link between nanobubbles and macroscopically observable electrokinetic phenomena *via* AFM, and investigating other methods for generating nanobubbles, such as temperature and pressure cycling.

Understanding these transient phenomena is critical for both electrokinetic characterization of hydrophobic microfluidic substrates, and for the design and operation of microfluidic devices fabricated from hydrophobic substrates. The ζ-potential measurements taken when the fluid–solid interface has not reached equilibrium may be inflated and therefore misleading. Furthermore, since many devices rely on solvent cycling, temperature cycling, and changing flow conditions, transient electrokinetic properties induced by fluctuating interfacial conditions may lead to an unexpected behavior.

The authors acknowledge our funding sources: Sandia National Labs (DOE PECASE) and ACS-PRF. They also thank Aditya N. Sharma for the useful discussions and his help in developing a correction factor for phase lag in phase-sensitive streaming potential experiments, Wyatt C. Nelson for his help in developing the automated current monitoring techniques, as well as Jonathan Posner (Arizona State) and Blake A. Simmons (Sandia National Labs) for useful discussions.

The authors have declared no conflict of interest.

6 References

[1] Mela, P., van den Berg, A., Fintschenko, Y., Cummings, E. B., Simmons, B. A., Kirby, B. J., *Electrophoresis* 2005, *26*, 1792–1799.

[2] Stone, H. A., Stroock, A. D., Ajdari, A., *Annu. Rev. Fluid Mech.* 2004, *36*, 381–411.

[3] McDonald, J. C., Duffy, D. C., Anderson, J. R., Chiu, D. T., Wu, H., Schueller, O. J. A., Whitesides, G. M., *Electrophoresis* 2000, *21*, 27–40.

[4] Hawkins, B. G., Smith, A. E., Syed, Y. A., Kirby, B. J., *Anal. Chem.* 2007, *79*, 7291–7300.

[5] Gaudioso, J., Craighead, H. G., *J. Chromatogr. A.* 2002, *971*, 249–253.

[6] Kameoka, J., Craighead, H. G., Zhang, H., Henion, J., *Anal. Chem.* 2001, *73*, 1935–1941.

© 2009 WILEY-VCH Verlag GmbH & Co. KGaA, Weinheim

[7] Tan, A., Benetton, S., Henion, J. D., *Anal. Chem.* 2003, *75*, 5504–5511.

[8] Schutzner, W., Kenndler, E., *Anal. Chem.* 1992, *64*, 1991–1995.

[9] Werner, C., Korber, H., Zimmermann, R., Dukhin, S., Jacobasch, H., *J. Colloid Interface Sci.* 1998, *208*, 329–346.

[10] Locascio, L. E., Perso, C. E., Lee, C. S., *J. Chromatogr. A.* 1999, *857*, 275–284.

[11] Caslavska, J., Thormann, W., *J. Microcolumn Sep.* 2001, *13*, 69–83.

[12] Kirby, B. J., Hasselbrink, E. F., jr., *Electrophoresis* 2004, *25*, 203–213.

[13] Tandon, V., Bhagavatula, S. K., Nelson, W. C., Kirby, B. J., *Electrophoresis* 2008, *29*, 1092–1101.

[14] Hunter, R. J., *Zeta Potential in Colloid Science*, Academic Press, London 1981.

[15] Lauga, E., Brenner, M. P., Stone, H. A., *Microfluidics: The No-Slip Boundary Condition*, Springer, New York 2005.

[16] Tandon, V., Kirby, B. J., *Electrophoresis* 2008, *29*, 1102–1114.

[17] Lee, C. Y., McCammon, J. A., Rossky, P. J., *J. Chem. Phys.* 1984, *80*, 4448–4455.

[18] Grigera, J. R., Kalko, S. G., Fischbarg, J., *Langmuir* 1996, *12*, 154–158.

[19] Mamatkulov, S. I., Khabibullaev, P. K., Netz, R. R., *Langmuir* 2004, *20*, 4756–4763.

[20] Joly, L., Ybert, C., Trizac, E., Bocquet, L., *Phys. Rev. Lett.* 2004, *93*, 257805.

[21] Vrbka, L., Mucha, M., Minofar, B., Jungwirth, P., *Curr. Opin. Colloid Interface Sci.* 2004, *9*, 67.

[22] Zangi, R., Engberts, J. B. F. N., *J. Am. Chem. Soc.* 2005, *127*, 2272–2276.

[23] Huang, D. M., Cottin-Bizonne, C., Ybert, C., Bocquet, L., *Phys. Rev. Lett.* 2007, *98*, 177801.

[24] Huang, D. M., Cottin-Bizonne, C., Ybert, C., Bocquet, L., *Langmuir* 2007, *24*, 1442–1450.

[25] Poynor, A., Hong, L., Robinson, I. K., Granick, S., Zhang, Z., Fenter, P. A., *Phys. Rev. Lett.* 2006, *97*, 266101.

[26] Doshi, D. A., Watkins, E. B., Israelachvili, J. N., Majewski, J., *Proc. Natl. Acad. Sci.* 2005, *102*, 9458–9462.

[27] Dang, L. X., Chang, T., *J. Phys. Chem. B.* 2002, *106*, 235–238.

[28] Attard, P., Moody, M. P., Tyrell, J. W. G., *Physica A.* 2002, *314*, 696–705.

[29] Attard, P., *Langmuir* 1996, *12*, 1693–1695.

[30] Attard, P., *Langmuir* 2000, *16*, 4455–4466.

[31] Attard, P., *Adv. Colloid Interface Sci.* 2003, *104*, 75–91.

[32] Hunter, R. J., *Foundations of Colloid Science*, Vol. 2, Clarendon Press, Oxford 1989.

[33] Lyklema, J., *Fundamentals of Interface and Colloid Science, Volume II: Solid–Liquid Interfaces*, Academic Press, London 1995.

[34] Kirby, B. J., Hasselbrink, E. F., Jr., *Electrophoresis* 2004, *25*, 187–202.

[35] Huang, X., Gordon, M. J., Zare, R.N., *Anal. Chem.* 1988, *60*, 1837–1838.

[36] Ross, D., Locascio, L. E., *Anal. Chem.* 2003, *75*, 1218–1220.

[37] Kirby, B. J., Reichmuth, D. S., Renzi, R. F., Shepodd, T. J., Wiedenman, B. J., *Lab Chip* 2005, *5*, 184–190.

[38] Ilic, B., Czaplewski, D., Neuzil, P., Stanczyk, T., Blough, J., Maclay, G. J., *J. Mater. Sci.* 2000, *38*, 3447–3457.

[39] Zhang, X. H., Maeda, N., Craig, Vincent, S. J., *Langmuir* 2006, *22*, 5025–5035.

[40] Liu, Y., Fanguy, J. C., Bledsoe, J. M., Henry, C. S., *Anal. Chem.* 2000, *72*, 5939–5944.

[41] Ocvirk, G., Munroe, M., Tang, T., Oleschuk, R., Westra, K., Harrison, D. J., *Electrophoresis* 2000, *21*, 107–115.

[42] Sze, A., Erickson, D., Ren, L., Li, D., *J. Colloid Interface Sci.* 2003, *261*, 402–410.

[43] Lacher, N. A., de Rooij, N. F., Verpoorte, E., Lunte, S. M., *J. Chromatogr. A.* 2003, *1004*, 225–235.

[44] Badal, M. Y., Wong, M., Chiem, N., Salimi-Moosavi, H., Harrison, D. J., *J. Chromatogr. A.* 2002, *947*, 277–286.

[45] Roberts, M. A., Rossier, J. S., Bercier, P., Girault, H., *Anal. Chem.* 1997, *69*, 2035–2042.

[46] Barker, S. L. R., Tarlov, M. J., Canavan, H., Hickman, J. J., Locascio, L. E., *Anal. Chem.* 2000, *72*, 4899–4903.

[47] Voigt, A., Wolf, H., Lauckner, S., Neumann, G., Becker, R., Richter, L., *Biomaterials* 1983, *4*, 299–304.

[48] Bianchi, F., Wagner, F., Hoffmann, P., Girault, H. H., *Anal. Chem.* 2001, *73*, 829–836.

[49] Reijenga, J. C., Aben, G. V. A., Verheggen, T. P. E. M., Everaerts, F. M., *J. Chromatogr.* 1983, *260*, 241–254.

[50] Lukacs, K. D., Jorgenson, J. W., *J. High Resolut. Chromatogr.* 1985, *8*, 407–411.

[51] Lappan, U., Buchhammer, H.-M., Lunkwitz, K., *Polymer.* 1999, *40*, 4087–4091.

[52] Huang, T.-L., *Chromatographia* 1993, *35*, 395–398.

[53] Scales, P. J., Grieser, F., Healy, T. W., *Langmuir* 1992, *8*, 965–974.

[54] Kosmulski, M., Matijevic, E., *Langmuir* 1992, *8*, 1060–1064.

[55] Dickens, J. E., Gorse, J., Everhart, J. A., Ryan, M., *J. Chromatogr. B.* 1994, *657*, 401–407.

[56] Ishida, N., Inoue, T., Miyahara, M., Higashitani, K., *Langmuir* 2000, *16*, 6377–6380.

[57] Lou, S., Gao, J., Xiao, X., Li, X., Li, G., Zhang, Y., Li, M. *et al.*, *Mater. Charact.* 2002, *48*, 211–214.

[58] Tyrrell, J. W. G., Attard, P., *Phys. Rev. Lett.* 2001, *87*, 176104.

[59] Tyrrell, J. W. G., Attard, P., *Langmuir* 2002, *18*, 160–167.

[60] Fischer, K., Wilken, M., *J. Chem. Thermodynamics* 2001, *33*, 1285–1308.

[61] Ljunggren, S., Eriksson, J. C., *Colloids Surf. A* 1997, *130*, 151–155.

[62] Schwer, C., Kenndler, E., *Anal. Chem.* 1991, *63*, 1801–1807.

© 2009 WILEY-VCH Verlag GmbH & Co. KGaA, Weinheim